PAPER

Check for updates

Dual-responsive near-infrared turn-on fluorescent probe for cancer stem cell-specific visualization†

Koji Miki, [iD] *[a] Masahiro Oe,[a] Kanae Suzuki,[a] Koki Miki,[a] Huiying Mu, [iD] [a] Yoshimi Kato,[b] Mayumi Iwatake,[b] Hiroshi Yukawa, [iD] [bcd] Yoshinobu Baba,[bc] Yoshifumi Ueda,[e] Yasuo Mori[e] and Kouichi Ohe [iD] *[a]

Aldehyde dehydrogenase 1A1 (ALDH1A1) stands out as one of the most reliable intracellular biomarkers for stem cells because it is expressed in both cancer stem cells (CSCs) and normal somatic stem cells (NSCs). Although several turn-on fluorescent probes for ALDH1A1 have been developed to visualize CSCs in cancer cells, the discrimination of CSCs from NSCs is difficult. We here report an AND-type dual-responsive fluorescent probe, **CHO_βgal**, the near-infrared fluorescence of which can be turned on after responding to both ALDH1A1 and β-galactosidase. The AND-type dual responsiveness enables CSCs to be clearly visualized, whereas NSCs are non-emissive in microscopy. CSC-positive metastasis model lungs were successfully discriminated from normal lungs in *ex vivo* staining experiments using **CHO_βgal**, whereas the single-input ALDH1A1-responsive probe failed to achieve this discrimination owing to pronounced false-positive fluorescence output from lung NSCs. In tissue slice staining experiments, even in the presence of adjacent normal tissues, the peripheral region-specific localization of CSCs was clear. The versatility of **CHO_βgal** holds promise not only as a fundamental *in vitro* research tool for visualizing CSCs but also as a valuable asset in practical tissue staining diagnosis, significantly contributing to the assessment of cancer malignancy.

Introduction

Cancer stem cells (CSCs) have generated great excitement in the research area of cancer because these cells are closely related to cancer initiation, progression, metastasis, and recurrence.[1–3] CSCs are a small population of cancer cells that present specific antigens on the surface and/or express specific intracellular enzymes.[4] During the past few decades, the CSC concept,[1–3] cancer plasticity,[5–8] and dormant cancer stem cells[6,9,10] have been intensively discussed in the field of oncology in an effort to understand the therapeutic response of cancers. Given that details of cancer progression and metastasis mechanisms

remain controversial, the development of reliable molecular imaging probes that can be used both to achieve a deeper understanding of CSCs and as a more efficient imaging agent for rapid and facile cancer malignancy assessment in clinical diagnosis, is highly desired. CSC fluorescence imaging is recognized as one of the most powerful tools because of its technical simplicity, noninvasive nature, and high spatiotemporal resolution.[11,12]

Intracellular enzyme aldehyde dehydrogenase 1A1 (ALDH1A1)[13,14] is one of the most promising biomarkers overexpressed in CSCs, and a variety of ALDH1A1-specific fluorescent probes have been developed to date.[11] The always-on fluorescent probe ALDEFLUOR[15] and analogous derivatives[16–18] are frequently used for CSC isolation based on fluorescence-activated cell sorting. Recently, turn-on fluorescent probes,[19–24] which are non-emissive before ALDH1A1-mediated transformation, have been developed for both visualization and isolation of CSCs in cancer cells. Some of the near-infrared (NIR) turn-on fluorescent probes were successfully applied to CSC-specific visualization *in vivo* and *ex vivo*.[20,22] However, ALDH1A1 is known to be an intracellular biomarker of stem cells and it is overexpressed both in CSCs in cancer tissues and normal somatic stem cells (NSCs) in normal tissues (Fig. 1(A)).[14,25,26] Hence, the discrimination of CSCs from NSCs is considered to be difficult by using single-input ALDH1A1-responsive probes (Fig. 1(B)). Given that

[a] Department of Energy and Hydrocarbon Chemistry, Graduate School of Engineering, Kyoto University, Katsura, Nishikyo-ku, Kyoto 615-8510, Japan. E-mail: kojimiki@scl.kyoto-u.ac.jp, ohe@scl.kyoto-u.ac.jp

[b] Institute of Nano-Life-Systems, Institutes of Innovation for Future Society, Nagoya University, Furo-cho, Chikusa-ku, Nagoya 464-8603, Japan

[c] Institute of Quantum Life Science, Quantum Life and Medical Science Directorate, National Institutes for Quantum Science and Technology (QST), Anagawa 4-9-1, Inage-ku, Chiba 263-8555, Japan

[d] Department of Quantum Life Science, Graduate School of Science, Chiba University, Chiba 265-8522, Japan

[e] Department of Synthetic Chemistry and Biological Chemistry, Graduate School of Engineering, Kyoto University, Katsura, Nishikyo-ku, Kyoto 615-8510, Japan

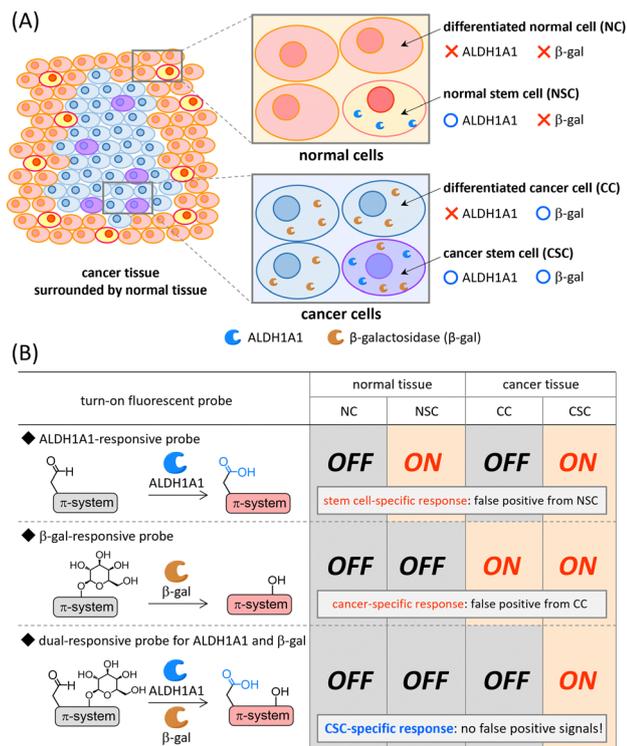† Electronic supplementary information (ESI) available. See DOI: https://doi.org/10.1039/d4tb00897a

This journal is © The Royal Society of Chemistry 2024

J. Mater. Chem. B, 2024, **12**, 6959–6967 | **6959**

Fig. 1 (A) ALDH1A1 and β-galactosidase (β-gal) expression in normal and cancer tissues. (B) Turn-on properties of ALDH1A1-responsive, β-galactosidase-responsive, and dual-responsive AND-type probes for CSC-specific visualization.

contamination of NSCs is usually unavoidable in surgically excised cancer tissues, a smart probe that becomes emissive in CSCs but remains silent in NSCs is urgently needed for the evaluation of cancer malignancy both in fundamental science and clinical diagnosis/therapy.[27]

Recently, dual-responsive fluorescent probes that can respond to two concurrently generated biological stimuli have been developed.[28] Among dual-responsive probes, AND-type probes can suppress false positive signals induced by one of two target stimuli. It is known that the expression level of β-galactosidase is upregulated in a wide range of cancer cells (Fig. 1(A));[29,30] therefore, a variety of β-galactosidase-responsive fluorescent probes have been developed for cancer detection.[31–34] Despite their cancer-specific identification, the discrimination of CSCs from differentiated cancer cells is considered to be difficult (Fig. 1(B)). Based on this background, we envisioned that a dual-responsive AND-type probe that becomes emissive only after both ALDH1A1- and β-galactosidase-mediated transformations would make specific visualization of CSCs possible (Fig. 1(B)). We herein report a dual-responsive turn-on fluorescent probe **CHO_βgal** (Fig. 2(A)), in which an NIR fluorescent hemicyanine dye is modified with both ALDH1A1- and β-galactosidase-responsive substrates. In *in vitro* cell staining using **CHO_βgal**, CSCs in cancer cells were specifically visualized with high contrast, whereas NSCs in normal cells remained non-emissive. In **CHO_βgal** staining of excised tissue slices, CSCs in cancer tissues as well as
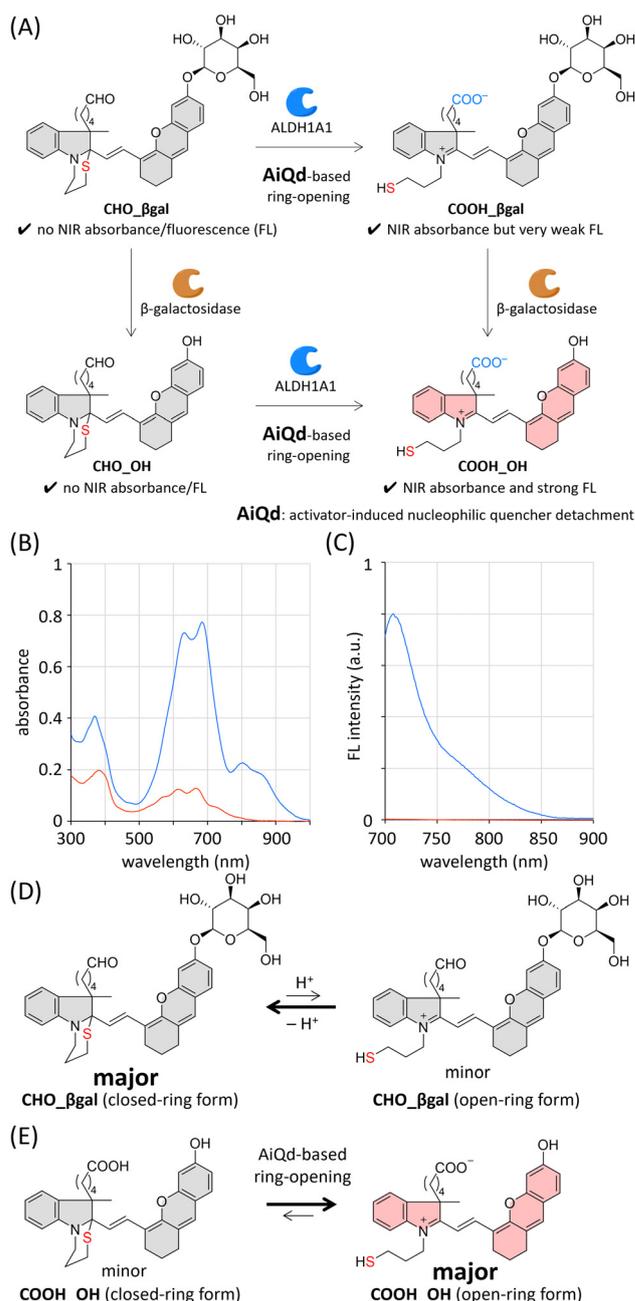

Fig. 2 (A) Dual-responsive AND-type fluorescent probe **CHO_βgal**. (B) Absorption and (C) fluorescence spectra of **CHO_βgal** (red) and **COOH_OH** (blue) in PBS (20 μM, pH 7.4, 1% DMSO). λ_{ex} = 680 nm. The equilibrium between open- and closed-ring forms of (D) **CHO_βgal** and (E) **COOH_OH**.

CSCs invading normal tissues were visualized even in the presence of NSCs.

Results and discussion

Probe design

To construct dual-responsive probe **CHO_βgal**, a member of the hemicyanine dye family, [2-((*E*)-2-(6-hydroxy-2,3-dihydro-1*H*-xanthen-4-yl)ethenyl)-3*H*-indol-1-ium], was selected as a

6960 | *J. Mater. Chem. B*, 2024, **12**, 6959–6967

This journal is © The Royal Society of Chemistry 2024

fluorophore, the NIR emission of which is suitable for both *in vitro* and *ex vivo* applications.[35,36] The NIR emission of the hemicyanine fluorophore is derived from its acceptor–π–donor structure consisting of an electron-accepting iminium group and an electron-donating phenolate moiety. Hence, its fluorescence emission can be quenched by modifying either of these two groups. The ALDH1A1-responsive molecular structure in **CHO_βgal** consists of an *N*-substituted benzoindole, an ω-formylbutyl group as an ALDH1A1 substrate, and an ω-mercaptopropyl group as a nucleophilic fluorescence quencher. Before the ALDH1A1-mediated oxidation of a formyl group, the intramolecular cyclization of the nucleophilic mercapto group takes place to form a 1,3-thiazinane ring structure under physiological conditions. Because the electron-accepting iminium group is masked by the mercapto group through this cyclization, it can be expected that **CHO_βgal** does not show NIR absorbance/fluorescence. After ALDH1A1-mediated transformation, the resulting carboxy group acts as an activator to promote ring-opening of the 1,3-thiazinane to generate an iminium group, thereby recovering the inherent π-extended dye skeleton. This activator-induced nucleophilic quencher detachment (AiQd) mechanism has been developed by us for enzyme-responsive turn-on fluorescent probes.[37,38] However, the electron-donating phenolate moiety remains capped with a weakly electron-donating β-galactosyl group after the sequential ALDH1A1-mediated transformation of **CHO_βgal** and AiQd-based ring-opening; therefore, it can be expected that the plausible product **COOH_βgal** has NIR absorbance but emits very weak NIR fluorescence. In the case of β-galactosidase-mediated transformation, **CHO_βgal** can be hydrolysed at the anomeric position of the β-galactosyl group to afford **CHO_OH**. Given that the 1,3-thiazinane ring is stable under physiological conditions, **CHO_OH** is assumed to show neither NIR absorbance nor fluorescence. After both ALDH1A1- and β-galactosidase-mediated transformations of **CHO_βgal**, the plausible product **COOH_OH** is expected to exhibit strong fluorescence.

Based on this design strategy, we prepared **CHO_βgal** as a dual-responsive AND-type turn-on fluorescent probe together with the plausible products **COOH_βgal**, **CHO_OH**, and **COOH_OH** (Schemes S1–S3 and Fig. S1–S3, ESI†). Because the closed-ring form of **CHO_βgal** contains two chiral quaternary carbons, it is formed as a mixture of major and minor diastereoisomers. Density functional theory (DFT) calculations support the conclusion that the ω-formylbutyl group and the 2-(6-galactosyl-2,3-dihydro-1*H*-xanthenyl)ethenyl group are located on the same side in the major diastereoisomer (Fig. S4, ESI†).

Photophysical properties

Absorption and fluorescence spectra of **CHO_βgal** and **COOH_OH** in neutral phosphate buffered solution (PBS, pH 7.4) were measured (Fig. 2(B), (C) and Table S1, ESI†). In the case of **CHO_βgal**, two broad signals were observed at 300–400 nm and 500–800 nm. As supported by time-dependent DFT calculations (Fig. S5, ESI†), the former absorbance is attributed to the closed-ring form in which the π-system is shortened. Because the

intramolecular nucleophilic cyclization of a mercapto group is a reversible reaction, the open-ring form of **CHO_βgal** was also present (Fig. 2(D)). Therefore, the latter absorbance can be assigned to a hemicyanine dye skeleton in the open-ring form. The molar extinction coefficients (ε, L mol^{-1} cm^{-1}) of **CHO_βgal** are 1.2×10^4 at 381 nm, 7.6×10^3 at 614 nm, and 7.3×10^3 at 667 nm. The ε value at 667 nm attributed to the open-ring form is much lower than those of common water-soluble hemicyanine dyes ($\varepsilon = \sim 3 \times 10^4$),[39] indicating that the closed-ring form of **CHO_βgal** is a major component in the solution. As expected, almost no NIR emission was detected in the fluorescence spectra. In contrast to **CHO_βgal**, **COOH_OH** showed strong absorbance at 600–700 nm ($\varepsilon = 3.5 \times 10^4$ at 681 nm), indicating that the AiQd mechanism is applicable to a hemicyanine skeleton and that the equilibrium of **COOH_OH** shifts to the open-ring form under neutral conditions (Fig. 2(E)). The broad absorbance around 800 nm can be assigned to the J-aggregate of the hemicyanine dye.[40] The fluorescence intensity of **COOH_OH** at 710 nm was more than 400 times stronger than that of **CHO_βgal**. We confirmed that both **CHO_OH** and **COOH_βgal** were slightly emissive but that the intensities were much weaker than that of **COOH_OH** (Fig. S6(A), ESI†). Because both the 1,3-thiazinane and phenolate moieties were expected to be pH-responsive, the pH-dependent spectral changes were investigated (Fig. S6–S9, ESI†). Although fluorescence intensity was dependent on pH values, it was confirmed that **COOH_OH** tends to be much more emissive than the other compounds under physiological conditions. By considering the photophysical properties of the compounds, **CHO_βgal** is expected to act as an AND-type turn-on fluorescent probe for ALDH1A1 and β-galactosidase.

Enzyme responsiveness

The AND-type dual responsiveness of **CHO_βgal** to enzymes was examined. In the absence of enzymes, no clear increase in fluorescence intensity was detected (Fig. 3(A)). A buffered aqueous solution of **CHO_βgal** (20 μM, pH 7.4) was incubated with ALDH1A1 (200 nM) and its fluorescence intensity was monitored. The broad peak at 700–750 nm in the fluorescence spectrum increased gradually during incubation and a peak at 710 nm (excitation: 660 nm) was detected that became 4.4 times stronger after 3 h incubation (Fig. 3(B) and (E)). As described in the previous section, **COOH_βgal** was slightly emissive because AiQd-based ring-opening shifts the equilibrium to its open-ring form. Hence, the weak NIR fluorescence output after ALDH1A1-mediated transformation is reasonable. When ALDH1A1 was pretreated with its inhibitor disulfiram and incubated with **CHO_βgal**, the increase in fluorescence intensity was suppressed, explaining the need for a formyl group (Fig. S10, ESI†). When the β-galactosidase-mediated transformation of **CHO_βgal** was examined, the fluorescence intensity was found to increase 4.3 times after 3 h incubation (Fig. 3(C) and (E)). The formation of weakly emissive **CHO_OH** was confirmed by liquid chromatography-mass spectroscopy (LC-MS) (Fig. S11, ESI†). The presence of an excess amount of D-galactose, which is a potent capping agent of the β-galactosidase active site,

This journal is © The Royal Society of Chemistry 2024
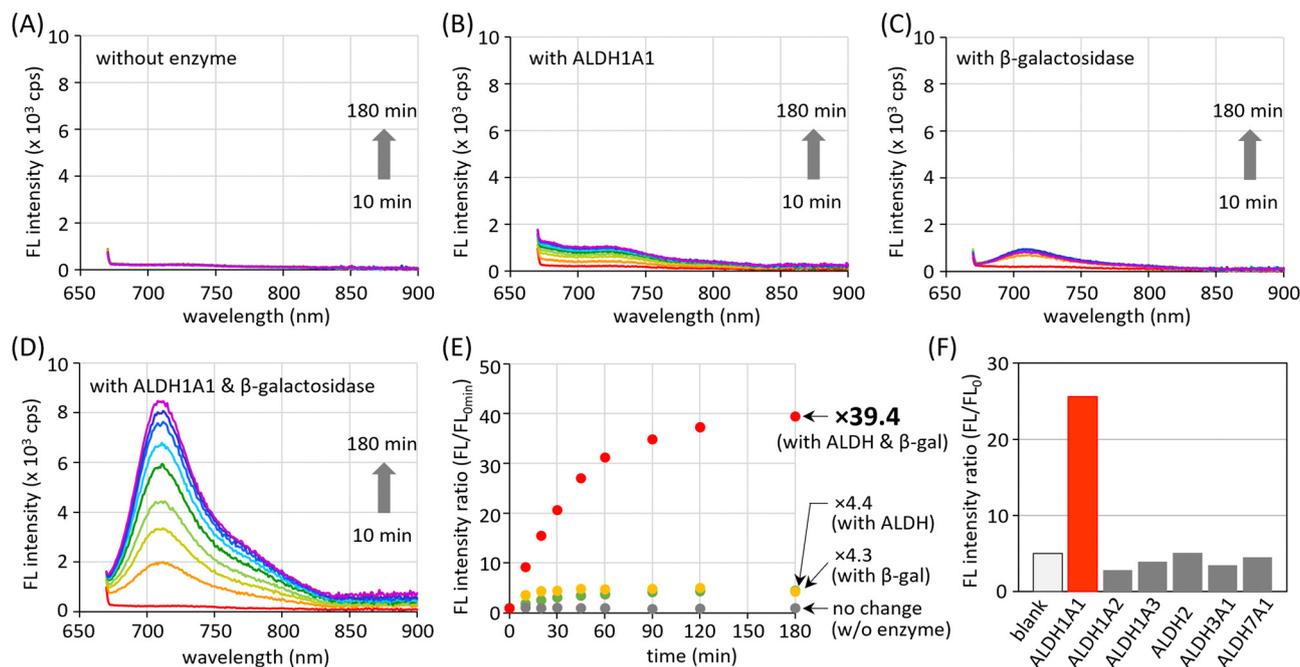
J. Mater. Chem. B, 2024, **12**, 6959–6967 | **6961**

Fig. 3 Time-dependent fluorescence change of **CHO_βgal** (20 μM) treated (A) without enzyme or with (B) ALDH1A1 (200 nM), (C) β-galactosidase (20 U mL^{-1}), and (D) both ALDH1A1 and β-galactosidase. (E) Time-dependent fluorescence intensity change of **CHO_βgal** (20 μM) at 710 nm (λ_{ex} = 660 nm) treated with ALDH1A1 (200 nM) and/or β-galactosidase (20 U mL^{-1}). (F) Fluorescence intensity of **CHO_βgal** at 710 nm (λ_{ex} = 660 nm) after incubation with ALDH isoforms (50 nM) for 120 min.

suppressed the increase in the fluorescence intensity (Fig. S12, ESI†). The increase of the fluorescence intensity after treatment of **CHO_βgal** with both ALDH1A1 and β-galactosidase was then monitored. LC-MS analysis after 1 h incubation confirmed that **CHO_βgal** was fully consumed and that both **COOH_βgal** and **COOH_OH** were generated (Fig. S13, ESI†). The fluorescence intensity was gradually increased to 39.4 times after 3 h incubation (Fig. 3(D) and (E)). These results indicate that the treatment of both ALDH1A1 and β-galactosidase smoothly generates emissive **COOH_OH** and that there is no significant interference between the two enzymes. Thus, the AND-type turn-on property of **CHO_βgal** mediated by ALDH1A1 and β-galactosidase was demonstrated. The limits of detection for ALDH1A1 and β-galactosidase were estimated at 1.7 μM and 0.032 U mL^{-1}, respectively, by measuring fluorescence intensities at different concentrations (Fig. S14, ESI†).

The stability of **CHO_βgal** under physiological conditions was examined (Fig. S15, ESI†). The fluorescence intensities after treatment of **CHO_βgal** with biological thiols such as cysteine, glutathione (GSH), and mercapto-containing protein (bovine serum albumin: BSA) were much weaker than that observed when **CHO_βgal** was incubated with both enzymes. Treatment of **CHO_βgal** with either amino acids bearing other functional groups or reactive oxygen species that oxidize a sulfur atom did not lead to fluorescence turn-on. Given that human ALDHs are found in 19 isoforms, the isoform selectivity of **CHO_βgal** was also examined. To this end, **CHO_βgal** was treated with several ALDH isoforms in the presence of β-galactosidase. As shown in Fig. 3(F), no significant increase

in fluorescence intensity was observed upon incubation with any of the representative ALDH isoforms (ALDH1A2, ALDH1A3, ALDH2, ALDH3A1, or ALDH7A1), indicating the pronounced high selectivity to ALDH1A1.

In vitro CSC visualization

To verify the dual responsiveness of **CHO_βgal** *in vitro*, human pancreatic carcinoma cell line SUIT-2 and human gastric signet ring carcinoma cell line KATO-III, both of which are known to contain CSCs with high ALDH1A1 activity, were treated with **CHO_βgal** (Fig. 4 and Fig. S18, ESI†).[30,41,42] Mouse embryonic fibroblast cell line NIH3T3 and human umbilical vein endothelial cell line HUVEC were chosen as representative β-galactosidase-negative normal cells for control experiments. To demonstrate the superiority of dual responsiveness, single-input ALDH1A1-responsive fluorescent probe **C5S-A**[22] was used as a control molecule. Based on the ALDEFLUOR assay,[15] we verified that NIH3T3 and HUVEC cells contain 11% and 33% ALDH1-positive cells, respectively (Fig. S22, ESI†). After treatment of SUIT-2 cells with **C5S-A**, a small population of brightly emissive cells that could be assigned to CSCs was visualized (Fig. 4(A) and Fig. S18(A), ESI†). In addition, it was confirmed that another cancer cell KATO-III as well as normal cells NIH3T3 and HUVEC contained brightly emissive ALDH1A1-positive cells. These results clearly indicate that single-input probe **C5S-A** is not suitable for discriminating between CSCs and NSCs.

The high cell viability of both cancer and normal cells was confirmed after 24 h incubation with **CHO_βgal** (0.01–100 μM),
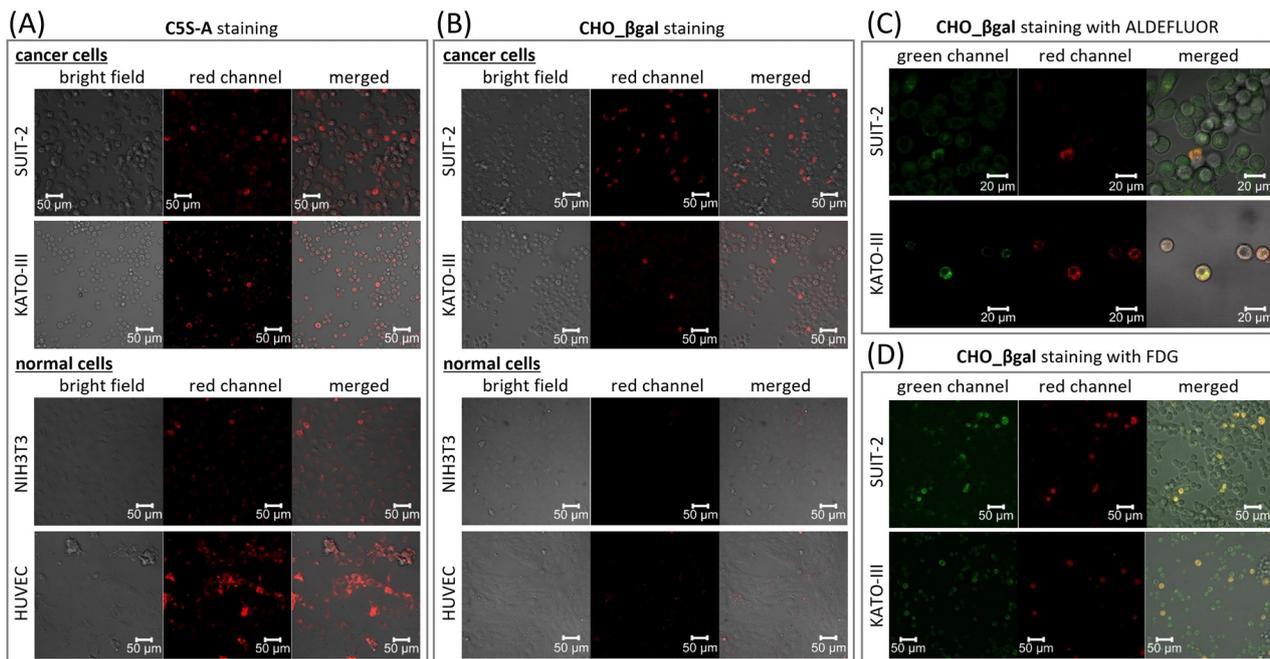
6962 | *J. Mater. Chem. B*, 2024, **12**, 6959–6967

This journal is © The Royal Society of Chemistry 2024

Fig. 4 Confocal laser scanning microscope images of SUIT-2, KATO-III, NIH3T3, and HUVEC cells stained with (A) **C5S-A** (1 μM) or (B) **CHO_βgal** (20 μM) without a washing step. Confocal laser scanning microscope images of SUIT-2 and KATO-III cells co-stained with **CHO_βgal** (20 μM) with (C) ALDEFLUOR (1 μM) or (D) FDG (20 μM). Green channel: λ_{ex} = 488 nm (λ_{det} = 500–600 nm); red channel: λ_{ex} = 633 nm (λ_{det} = 647–759 nm).

indicating that **CHO_βgal** has low cytotoxicity at a concentration of < 20 μM (Fig. S16, ESI†). We next examined the turn-on nature of **CHO_βgal** in both cancer and normal cells. Cancer cell staining using **CHO_βgal** resulted in brightly emissive cells being observed together with a large number of non-emissive cells (Fig. 4(B) and Fig. S18(B), ESI†). Notably, no washing step was necessary to obtain high-contrast visualization because of the turn-on property of **CHO_βgal**. Furthermore, the signal/noise ratios (F_{CSC}/F_{CC}) of **CHO_βgal**, which were obtained by dividing the fluorescence intensities of CSCs (F_{CSC}) by those of differentiated cancer cells (F_{CC}), were 11.4 ± 2.0 for SUIT-2 and 15.4 ± 3.5 for KATO-III, which are much higher than those of **C5S-A** (F_{CSC}/F_{CC} = 4.4 ± 0.9 for SUIT-2 and 3.6 ± 1.3 for KATO-III) (Fig. S17, ESI†). The high signal/noise ratios suggest that **CHO_βgal** is a suitable probe for high contrast CSC visualization. It is noted that more than 10 μM of **CHO_βgal** should be used for clear staining because of lower fluorescence intensity of hemicyanine dyes compared with cyanine dyes. As shown in the enzymatic transformation experiments, conversion of **CHO_βgal** catalysed by either ALDH1A1- or β-galactosidase alone did not yield a strong fluorescence output; therefore, the strong fluorescence was obtained only through conversion of **CHO_βgal** catalysed by both enzymes. To confirm that the expression levels of ALDH1A1 and β-galactosidase are both upregulated in CSCs, co-staining experiments were conducted using **CHO_βgal** with green-fluorescent ALDEFLUOR or fluorescein di-β-D-galactopyranoside (FDG),[43,44] which is a commercial green-fluorescent β-galactosidase-specific single-input probe (Fig. 4(C), (D) and Fig. S19, ESI†). In low-magnification mode, ALDEFLUOR

staining did not clearly distinguish ALDH1-positive cells of SUIT-2 from ALDH1-negative cells because of its always-on nature. On the other hand, in higher magnification mode, slightly brighter cells were identified in the green channel and the cells were also emissive in the deep-red channel (Fig. 4(C) and Fig. S19(A), ESI†). In the case of KATO-III, brighter cells were identified in the green channel even in low magnification mode and the stained cells were the same as those seen in the deep-red channel (Fig. S20, ESI†). This is probably because the ALDH1A1 expression level in CSCs of KATO-III is higher than that of SUIT-2.[30] In co-staining experiments using **CHO_βgal** with FDG, **CHO_βgal**-positive cells were included in FDG-positive cells (Fig. 4(D), and Fig. S19(B), ESI†). Surprisingly, fluorescence from **CHO_βgal**-negative cells was observed in the green channel, but the intensity was significantly weaker than fluorescence from **CHO_βgal**-positive cells. The co-staining results strongly suggest that the β-galactosidase activity is upregulated in ALDH1A1-positive CSCs in both SUIT-2 and KATO-III. The use of **CHO_βgal** confirmed that FDG is an effective probe for detecting ALDH1A1-positive CSCs in specific cell lines. Pre-treatment of cells with either the ALDH1A1 inhibitor disulfiram or β-galactosidase competitive substrate D-galactose successfully suppressed the fluorescence turn-on of **CHO_βgal** (Fig. S21, ESI†). No positive images were observed with NIH3T3 and HUVEC (Fig. 4(B) and Fig. S18(B), ESI†), indicating that **CHO_βgal** can be used to successfully distinguish CSCs from NSCs *in vitro*. Flow cytometry analysis of HUVEC cells also supports that **CHO_βgal** remains silent in NSCs (Fig. S23, ESI†). These results suggest that **CHO_βgal** staining has the potential to selectively visualize/isolate CSCs

This journal is © The Royal Society of Chemistry 2024

J. Mater. Chem. B, 2024, **12**, 6959–6967 | **6963**

from tissues containing both normal and cancer cells harvested from patients. Furthermore, through co-staining experiments using commercial single-input probes, we found that the β-galactosidase expression levels in CSCs are clearly higher than those in differentiated cancer cells in specific cell lines. More importantly, these results suggest that the new design of dual-responsive probes for ALDH1A1 and other biological analytes will find new biomarkers that are specifically expressed in CSCs.

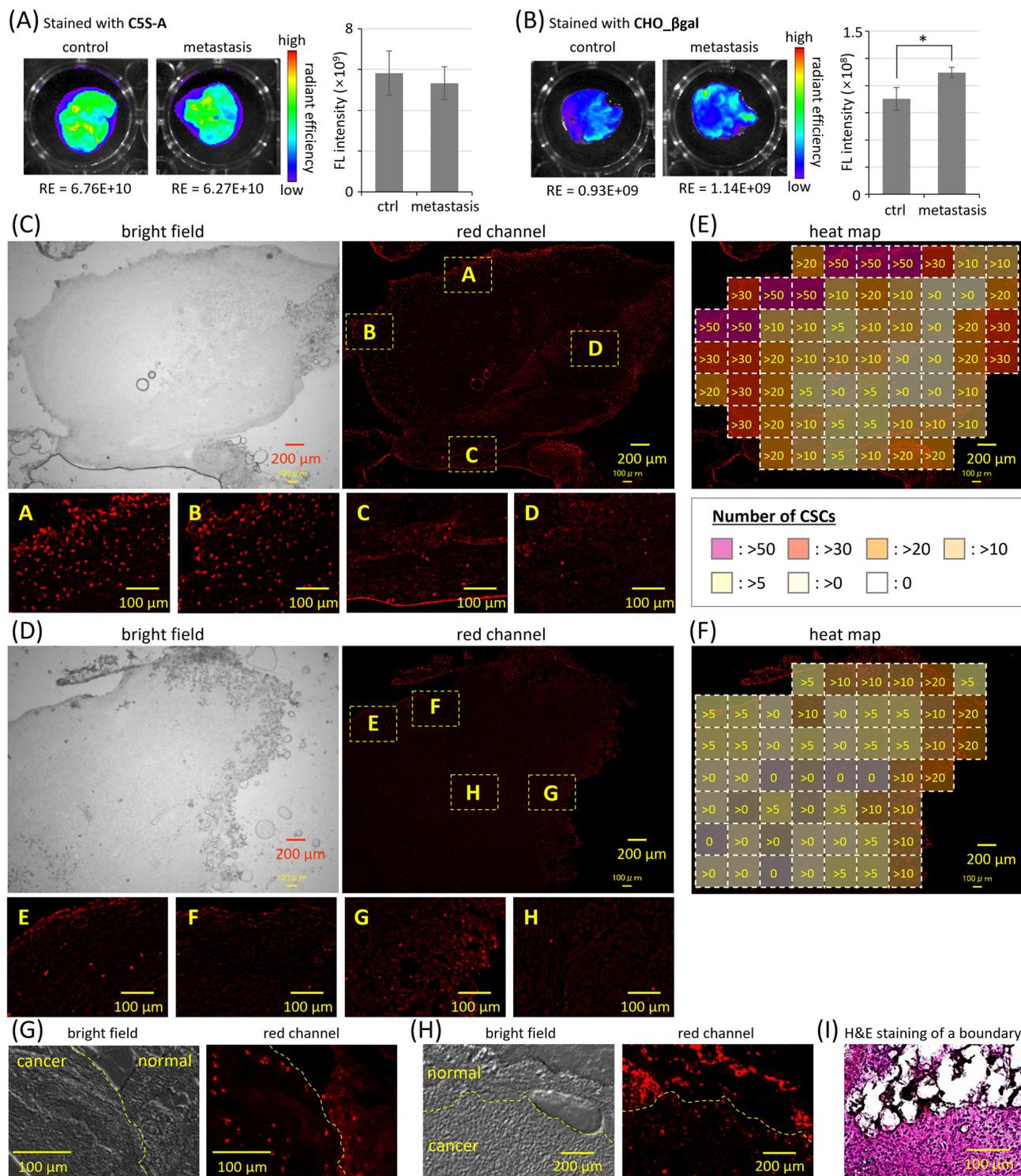### Ex vivo CSC visualization

In cancer metastasis, cancer cells break off from the original cancer tissues and spread to other organs; therefore, cancer metastasis is often associated with adverse prognoses. The invasion of CSCs through the basal membrane into blood vessels is proposed as one of the most plausible mechanisms of cancer metastasis initiation.[1–3] The intravenous injection of cancer cells into mice is a facile method to prepare model mice bearing metastatic cancer in the lungs,[45] in which the CSC population increases. The excised lungs of nude mice five days after intravenous injection of SUIT-2 cells were stained by using single-input probe **C5S-A** and dual-responsive probe **CHO_βgal** (Fig. 5 and Fig. S24, ESI†). The excised lungs of nude mice without injection of SUIT-2 cells were also stained for control experiments. In the case of **C5S-A**, strong fluorescence was observed in the lungs of both metastasis model mice and normal mice (Fig. 5(A) and Fig. S24(A), ESI†); there was no significant difference between these two groups. The strong fluorescence is considered to be caused by ALDH1A1 expressed in NSCs of lung tissues. In contrast, in the case of **CHO_βgal**, much weaker fluorescence was observed in both the control and metastasis lungs, indicating that **CHO_βgal** successfully suppresses the false-positive signals from NSCs (Fig. 5(B) and Fig. S24(B), ESI†). A significant difference between the two groups was confirmed; however, the difference in fluorescence intensities was not large. As shown in Fig. 3(E), the fluorescence intensity increments of **CHO_βgal** after the treatment either with only ALDH1A1 or with both ALDH1A1 and β-galactosidase were 4.4 times and 39.4 times, respectively. The number of NSCs in metastasis model lungs is expected to be much greater than that of CSCs. Although the difference in fluorescence intensity increments was clear in the enzyme treatment experiments, the fluorescence after conversion of **CHO_βgal** by ALDH1A1 in NSCs pushed up the background fluorescence, resulting in the small difference in fluorescence intensity between the metastasis model lungs and normal lungs.

Finally, by staining excised slices of both normal and cancer tissue, we evaluated the CSC staining ability of **CHO_βgal**. The normal and cancer tissues as well as the boundary region between these two tissues were identified by using hematoxylin and eosin (H&E) staining (Fig. 5(I) and Fig. S32, ESI†). No strong fluorescence was observed from adipose tissue slices, which were used as a normal tissue model with low β-galactosidase expression level (Fig. S25, ESI†). In cancer tissue slices, which were prepared by the intraperitoneal injection of

SUIT-2 cells into femoral subcutaneous adipose tissues of mice, much stronger fluorescence was detected from the entire tissue slice together with many bright spots (Fig. 5(C) and Fig. S26, ESI†). When cancer tissue slices were treated with a mixture of **CHO_βgal** and ALDH1A1 inhibitor disulfiram, the number of bright spots decreased significantly (Fig. 5(D) and Fig. S27, ESI†). Similar bright spots were observed in the cancer tissue slices stained by **C5S-A**; however, these spots were difficult to be discriminated because of the high background signal of **C5S-A** (Fig. S28, ESI†). The number of bright spots was also decreased under co-treatment of **C5S-A** with disulfiram (Fig. S29, ESI†). These results clearly indicate that the bright spots observed in both **CHO_βgal** and **C5S-A** staining arise from fluorescence from CSCs. The heat maps of the numbers of CSCs detected in Fig. 5(C) and (D) are summarized in Fig. 5(E) and (F), respectively. Interestingly, CSCs were localized in the peripheral region of cancer tissues, whereas almost no CSCs were detected in the core of the tissues. Considering that CSCs are closely related to cancer progression and metastasis,[46] it is reasonable to conclude that active CSCs are specifically localized at the peripheral region of cancer tissues. It is known that cancer tissues contain invasive leader cells, the so-called "leading front", having proliferative, invasive, and metastatic abilities compared with other trailing follower cells.[47] As shown in Fig. 5(E), it is obvious that the density of CSCs was higher at the left upper side, but lower at the lower side. This result suggests that **CHO_βgal** staining can point out the location of the active "leading front" in malignant cancer tissues.

Because CSCs in cancer tissue slices were successfully visualized, the discrimination of CSCs from NSCs in tissue slices was next examined. When a boundary region between cancer and adipose tissues was excised and the slices were stained with **CHO_βgal** (Fig. 5(G) and Fig. S30, ESI†), many bright spots were observed. It was confirmed that the ALDH1A1 inhibitor disulfiram successfully suppressed the fluorescence turn-on in the sliced tissues (Fig. S31, ESI†). The many bright spots that were assignable to CSCs were predominantly observed on the side of the cancer tissue near the boundary region. This observation is consistent with the distribution of stained cells in cancer tissue slices shown in Fig. 5(C). In the case of tissue slice staining using single-input probe **C5S-A**, many bright spots were observed in both cancer and adipose tissues (Fig. 5(H) and Fig. S28, ESI†) and the emission could be suppressed by ALDH1A1 inhibitor disulfiram (Fig. S29, ESI†). These results clearly indicate that the single-input probe could respond to ALDH1A1 in both CSCs and NSCs, being not suitable for CSC-specific visualization. In contrast, in the case of **CHO_βgal** staining, the CSC-specific visualization at the boundary region was not influenced by the presence of NSCs. These results strongly suggest that **CHO_βϖgal** staining will be applicable to practical cancer malignancy assessment using excised tissue slices that contain both cancer and normal tissues. Some bright spots were observed on the side of adipose tissues near the boundary region, probably indicating that **CHO_βgal** staining can reveal CSCs invading normal tissues.

6964 | *J. Mater. Chem. B*, 2024, **12**, 6959–6967

This journal is © The Royal Society of Chemistry 2024

Fig. 5 *Ex vivo* fluorescence images of excised lungs of mice stained by (A) **C5S-A** and (B) **CHO_βgal**. Metastasis model mice: SUIT-2 cell suspension was intravenously injected 5 days before lung excision. Radiant efficiency (RE): (photon per s cm^{-2} sr^{-1})/(μW cm^{-2}). * $p < 0.05$ ($n = 3$). Slices of cancer tissues stained by **CHO_βgal** (C) without or (D) with disulfiram. Yellow dashed squares A–H were enlarged. The distribution of CSCs in cancer tissue slices shown in Fig. (E) 5(C) and (F) 5(D) is summarized as a heat map. The numbers of CSCs in a region of interest are shown. Slice of the boundary region between cancer and adipose tissues stained by (G) **CHO_βgal** or (H) **C5S-A**. The boundary between cancer tissue and normal adipose tissue is shown as a yellow dashed line. $\lambda_{ex} = 620/60$ nm ($\lambda_{det} = 700/25$ nm). (I) Hematoxylin and eosin-stained slice of a boundary region.

This journal is © The Royal Society of Chemistry 2024

J. Mater. Chem. B, 2024, **12**, 6959–6967 | **6965**

Conclusions

In summary, we have developed the ALDH1A1- and β-galactosidase-responsive turn-on fluorescent probe **CHO_βgal** and applied it to *in vitro* and *ex vivo* CSC visualization. **CHO_βgal** was successfully synthesized by decorating hemicyanine dye with ALDH1A1 and β-galactosidase-responsive substrates. Both ALDH1A1- and β-galactosidase-mediated transformations gave the emissive **COOH_OH** from **CHO_βgal**, but neither of the two independent transformations yielded strong fluorescence. In *in vitro* confocal laser scanning microscopy observations, **CHO_βgal** clearly and selectively lit up CSCs in the presence of differentiated cancer cells. Thanks to the AND-type dual responsiveness of **CHO_βgal**, false-positive signals from NSCs were suppressed, which has not been attained with single-input ALDH1A1-responsive probes. As shown in *ex vivo* imaging of excised lungs, **CHO_βgal** can effectively avoid false-positive assignments, discriminating metastasis model lungs from normal lungs. The tissue slice staining using **CHO_βgal** elucidated that active CSCs localize at the peripheral region in cancer tissues and it was able to point out the invasive "leading front" in malignant cancer tissues. Furthermore, CSC-specific visualization in tissue slices was not disturbed by NSCs. To our knowledge, this is the first example of visualization of ALDH1A1-positive CSCs in surgically excised tissue slices containing NSCs. Hence, we believe that the **CHO_βgal** staining will become not only a reliable and facile diagnostic method for detecting CSC-positive cancer tissues and evaluating cancer malignancy, but also a powerful and promising tool for pursuing the origin of CSCs and cancer plasticity.

Author contributions

Koji M. and M. O. conceived and designed the study. Koji M., M. O., K. S., and Koki M. synthesized and characterized the compounds. Koji M., M. O., K. S., and H. M. performed *in vitro* cell experiments. Koji M. performed theoretical calculation. Koji M., M. O., Y. K., M. I, H. Y., Y. B., Y. U., and Y. M. performed *ex vivo* metastasis model lung staining. Y. K., M. I, H. Y., and Y. B. performed *ex vivo* tissue slice staining and H&E staining. K. O. directed the project. The manuscript was written by Koji M. and K. O.

Conflicts of interest

There are no conflicts to declare.

Acknowledgements

References

1 E. Batlle and H. Clevers, *Nat. Med.*, 2017, **23**, 1124–1134.
2 B. Beck and C. Blanpain, *Nat. Rev. Cancer*, 2013, **13**, 727–738.
3 Q. Gao, Y. Zhan, L. Sun and W. Zhu, *Stem Cell Rev. Rep.*, 2023, **19**, 2141–2154.
4 L. Walcher, A.-K. Kistenmacher, H. Suo, R. Kitte, S. Dluczek, A. Strauβ, A.-R. Blaudszun, T. Yevsa, S. Fricke and U. Kossatz-Boehlert, *Front. Immunol.*, 2020, **11**, 1280.
5 N. M. Warrier, N. Kelkar, C. T. Johnson, T. Govindarajan, V. Prabhu and P. Kumar, *Eur. J. Cell Biol.*, 2023, **102**, 151321.
6 R. Paul, J. F. Dorsey and Y. Fan, *Pharmcol. Ther.*, 2022, **231**, 107985.
7 P. B. Gupta, I. Pastushenko, A. Skibinski, C. Blanpain and C. Kuperwasser, *Cell Stem Cell*, 2019, **24**, 65–78.
8 C. E. Meacham and S. J. Morrison, *Nature*, 2013, **501**, 328–337.
9 M. L. De Angelis, F. Francescangeli, F. La Torre and A. Zeuner, *Front. Oncol.*, 2019, **9**, 626.
10 G. L. Ismaeel, A. H. Abdul-Hussein, H. M. Qasim, N. K. Abed, A. T. Jalil, A. A. Suleiman and S. H. Dilfy, *Gene Rep.*, 2023, **30**, 101717.
11 J. Han, M. Won, J. H. Kim, E. Jung, K. Min, P. Jangili and J. S. Kim, *Chem. Soc. Rev.*, 2020, **49**, 7856–7878.
12 H. Jariyal, C. Gupta, V. S. Bhat, J. R. Wagh and A. Srivastava, *Stem Cell Rev. Rep.*, 2019, **15**, 755–773.
13 X. Xu, S. Chai, P. Wang, C. Zhang, Y. Yang, Y. Yang and K. Wang, *Cancer Lett.*, 2015, **369**, 50–57.
14 H. Tomita, K. Tanaka, T. Tanaka and A. Hara, *Oncotarget*, 2016, **7**, 11018–11032.
15 R. W. Storms, A. P. Trujillo, J. B. Springer, L. Shah, O. M. Colvin, S. M. Ludeman and C. Smith, *Proc. Natl. Acad. Sci. U. S. A.*, 1999, **96**, 9118–9123.
16 I. Min, H. Wang, R. C. Mease, Y. Byun, X. Yang, J. Wang, S. D. Leach and M. G. Pomper, *Nat. Commun.*, 2014, **5**, 3662.
17 A. Yagishita, T. Ueno, H. Esumi, H. Saya, K. Kaneko, K. Tsuchihara and Y. Urano, *Bioconjugate Chem.*, 2017, **28**, 302–306.
18 A. Yagishita, T. Ueno, K. Tsuchihara and Y. Urano, *Bioconjugate Chem.*, 2021, **32**, 234–238.
19 S. Maity, C. M. Sadlowski, J.-M. G. Lin, C.-H. Chen, L.-H. Peng, E.-S. Lee, G. K. Vegesna, C. Lee, S. H. Kim, D. Mochly-Rosen, S. Kumar and N. Murthy, *Chem. Sci.*, 2017, **8**, 7143–7151.
20 C. Anorma, J. Hedhli, T. E. Bearrood, N. W. Pino, S. H. Gardner, H. Inaba, P. Zhang, Y. Li, D. Feng, S. E. Dibrell, K. A. Kilian, L. W. Dobrucki, T. M. Fan and J. Chan, *ACS Cent. Sci.*, 2018, **4**, 1045–1055.

6966 | *J. Mater. Chem. B*, 2024, **12**, 6959–6967

This journal is © The Royal Society of Chemistry 2024

21 T. E. Bearrood, G. Aguirre-Figueroa and J. Chan, *Bioconjugate Chem.*, 2020, **31**, 224–228.

22 M. Oe, K. Miki, Y. Ueda, Y. Mori, A. Okamoto, Y. Funakoshi, H. Minami and K. Ohe, *ACS Sens.*, 2021, **6**, 3320–3329.

23 M. Oe, K. Suzuki, K. Miki, H. Mu and K. Ohe, *ChemPlusChem*, 2022, **87**, e202200319.

24 S. Li, W. Tang and X. Duan, *New J. Chem.*, 2023, **47**, 545–549.

25 I. Ma and A. L. Allan, *Stem Cell Rev. Rep.*, 2011, **7**, 292–306.

26 G. Vassalli, *Stem Cell Inter.*, 2019, **2019**, 3904645.

27 F. Rossi, H. Noren, R. Jove, V. Beljanski and K.-H. Grinnemo, *Stem Cell Res. Ther.*, 2020, **11**, 489.

28 J. L. Kolanowski, F. Liu and E. J. New, *Chem. Soc. Rev.*, 2018, **47**, 195–208.

29 D. H. Juers, B. W. Matthews and R. E. Huber, *Protein Sci.*, 2012, **21**, 1792–1807.

30 A. Tsherniak, F. Vazquez, P. G. Montgomery, B. A. Weir, G. Kryukov, G. S. Cowley, S. Gill, W. F. Harrington, S. Pantel, J. M. Krill-Burger, R. M. Meyers, L. Ali, A. Goodale, Y. Lee, G. Jiang, J. Hsiao, W. F. J. Gerath, S. Howell, E. Merkel, M. Ghandi, L. A. Garraway, D. E. Root, T. R. Golub, J. S. Boehm and W. C. Hahn, *Cell*, 2017, **170**, 564–576.

31 J. Zhang, P. Cheng and K. Pu, *Bioconjugate Chem.*, 2019, **30**, 2089–2101.

32 Y. Yao, Y. Zhang, C. Yan, W.-H. Zhu and Z. Guo, *Chem. Sci.*, 2021, **12**, 9885–9894.

33 M. Li, M. Yang and W.-H. Zhu, *Mater. Chem. Front.*, 2021, **5**, 763–774.

34 L. Li, F. Jia, Y. Li and Y. Peng, *RSC Adv.*, 2024, **14**, 3010–3023.

35 H. Li, H. Kim, F. Xu, J. Han, Q. Yao, J. Wang, K. Pu, X. Peng and J. Yoon, *Chem. Soc. Rev.*, 2022, **51**, 1795–1835.

36 Z. Zeng, S. S. Liew, X. Wei and K. Pu, *Angew. Chem., Int. Ed.*, 2021, **60**, 26454–26475.

37 M. Oe, K. Miki and K. Ohe, *Org. Biomol. Chem.*, 2020, **18**, 8620–8624.

38 M. Oe, K. Miki, A. Masuda, K. Nogita and K. Ohe, *Chem. Commun.*, 2022, **58**, 1510–1513.

39 X.-P. Fam, J. Huang, T.-B. Ren, L. Yuan and X.-B. Zhang, *Anal. Chem.*, 2023, **95**, 1566–1573.

40 Z. Li, P.-Z. Liang, L. Xu, S.-S. Zhang, K. Li, Q. Wu, S.-F. Lou, T.-B. Ren, L. Yuan and S.-B. Zhang, *Nat. Commun.*, 2023, **14**, 1843.

41 Y. Hoshino, J. Nishida, Y. Katsuno, D. Koinuma, T. Aoki, N. Kokudo, K. Miyazono and S. Ehata, *Am. J. Pathol.*, 2015, **185**, 1457–1470.

42 Y. Katsuno, S. Ehata, M. Yashiro, K. Yanagihara, K. Hirakawa and K. Miyazono, *J. Pathol.*, 2012, **228**, 391–404.

43 B. Rotman, J. A. Zderic and M. Edelstein, *Proc. Natl. Acad. Sci. U. S. A.*, 1963, **50**, 1–6.

44 F. Debacq-Chainiaux, J. D. Erusalimsky, J. Campisi and O. Toussaint, *Nat. Protoc.*, 2009, **4**, 1798–1806.

45 N. Kitamura, T. Iwamura, S. Taniguchi, H. Yamanari, M. A. Kawano, K. Hollingworth and T. Setoguchi, *Clin. Exp. Metastasis*, 2001, **18**, 561–571.

46 Q. Li, Z. Guo, G. Li, Y. Zhang, X. Liu, B. Li, J. Wang and X. Li, *Cancer Cell Int.*, 2023, **23**, 305.

47 J.-s Wu, J. Jiang, B.-j Chen, K. Wang, Y.-l Tang and X.-h Liang, *Transl. Oncol.*, 2021, **14**, 100899.

This journal is © The Royal Society of Chemistry 2024

J. Mater. Chem. B, 2024, **12**, 6959–6967 | **6967**